J. Fluid Mech. (2014), *vol.* 758, *pp.* 312–326. © Cambridge University Press 2014
doi:10.1017/jfm.2014.531

Interfacial instabilities in sediment suspension flows

Maryam Abedi[1], **Mir Abbas Jalali**[1,2,†] **and Maniya Maleki**[3]

[1]Department of Mechanical Engineering, Sharif University of Technology, Azadi Avenue, Tehran, Iran

[2]Department of Astronomy, University of California, Berkeley, CA 94720-3411, USA

[3]Department of Physics, Institute for Advanced Studies in Basic Sciences, Zanjan 45137-66731, Iran

(Received 25 June 2014; revised 25 June 2014; accepted 5 September 2014;
first published online 8 October 2014)

We report the existence of interfacial instability in the two-dimensional channel flow of a sediment suspension whose particles diffuse in the carrier fluid due to shear-induced collisions. We derive partial differential equations that govern the deformations of the interface between the sediment suspension and the clear fluid, and devise a perturbation method that preserves the positivity of the particle volume fraction. We solve perturbed momentum, particle transport and deforming interface equations to show that a Kelvin–Helmholtz-type unstable wave develops at the interface for wavelengths longer than a critical value. Short-wavelength oscillations of the interface are damped due to shear-induced diffusion of particles. We also show that the lowest critical Reynolds number, above which the interface is unstable, occurs for intermediate values of the total volume fraction of particles.

Key words: instability, multiphase and particle-laden flows, suspensions

1. Introduction

When a sediment is sheared by a clear fluid, instabilities may occur at the interface. Sand ripples and dunes observed in shallow water or subaqueous flows are natural examples of this process. Mass transfer in food processing, transport of coal and dredging may also cause interfacial instabilities. Experimental set-ups are widely used to study interfacial instabilities in Couette flow (Lenoble, Snabre & Pouligny 2005), pressure-driven channel flow (Maleki *et al.* 2009), open-channel flow (Langlois & Valance 2007) and tube flow (Norman, Nayak & Bonnecaze 2005). On the theoretical side, the advancement in the modelling and understanding of interfacial waves has been mostly in problems with low Shields numbers, and the erodible bed concept has been used to model the variations of the sediment thickness. By solving viscous flow equations over the fixed bed (Charru & Mouilleron-Arnould 2002), the wavelengths of sand ripples and dunes (Valance & Langlois 2005) along with the mechanisms of instability (Kouakou & Lagrée 2005) have been investigated. In these studies the temporal evolution of the bedform is slow compared with the time scale of the flow. The assumption of a fixed or slowly varying bedform, however, is not valid when shear stresses at the bed overwhelm the force of gravity. Experimental studies of

† Email address for correspondence: mjalali@berkeley.edu

https://doi.org/10.1017/jfm.2014.531 Published online by Cambridge University Press

suspension flows have shown that the height of the mobile layer and its velocity are comparable with the height and velocity of the clear fluid, even for large values of particle density (Aussillous *et al.* 2013). Direct numerical simulations of sedimenting particles in Poiseuille flow have also shown that the velocities of the sediment layer and clear fluid are comparable at high Reynolds numbers (Papista, Dimitrakis & Yiantsios 2011). Therefore, the velocity of the sediment cannot be neglected.

There are few studies in the continuum limit that treat suspensions with fully mobile sediment and clear fluid components (Zhang, Acrivos & Schaflinger 1992; Schaflinger 1994; Kuru, Leighton & McCready 1995; Miskin, Elliott & Ingham 1999). These studies utilize the diffusive flux model and include gravitational forces to explore interfacial instabilities. Nonetheless, they all ignore the perturbation of the particle concentration ϕ within the sediment and at the interface. Moreover, the non-uniformity of ϕ in the initial steady-state flow has been considered only by Kuru *et al.* (1995) and Miskin *et al.* (1999). Neglect of the non-uniformity and disturbances of ϕ yields a problem almost analogous to the stability analysis of immiscible fluids, and we do not gain much information about the effect of particle diffusion/migration on interfacial instabilities.

The study of instabilities at the interface of two immiscible fluids and in different flow conditions has a long history (Yih 1967; Hooper & Boyd 1983; Yiantsios & Higgins 1988). Nonetheless, our knowledge about the consequences of sharp changes in physical properties, like viscosity and density, is limited. Experiments (Aussillous *et al.* 2013) and theoretical models (Miskin *et al.* 1996) show that the particle concentration and sediment properties gradually change, and the assumption of constant density and viscosity across the sediment is not justified, especially for high Shields numbers. Moreover, particle flux at the interface can mix two fluid layers and influence the development of interfacial waves. In order to model the gradual changes of properties at the interface, one may assume a miscible layer between two fluids (Govindarajan 2004; Talon & Meiburg 2011), but in most observed cases of sediment flow the variation of physical properties has occurred within the entire sediment layer and not part of it.

In this paper, we adopt the phenomenological model of Cook (2008), and study interfacial instabilities that emerge in the pressure-driven channel flow of a clear fluid over a heavier suspension whose particles are subject to shear-induced migration. We consider the non-uniformity of particle concentration in steady and perturbed states, and work with a fully mobile sediment layer. In § 2, we introduce the model, find steady-state solutions when the particle concentration profile within the sediment is non-uniform, and develop a new positivity-preserving perturbation theory that takes into account the variations of the sediment height and disturbances of $\phi \geqslant 0$. We then formulate an eigenvalue problem and carry out a linear stability analysis to trace the deformations of the interface. Exponentially growing interfacial waves and the effect of model parameters on their development are discussed in § 3. Our concluding remarks are presented in § 4.

2. Governing equations

We attempt to derive and solve the steady-state and disturbed governing equations of sediment suspension flows whose particles are spherical and are subject to shear-induced diffusion (SID). We assume that the suspension is incompressible and the particles are negatively buoyant. The volume fraction ϕ of particles within the sediment is large, but stays below the maximum value $\phi_m = 0.68$ for spherical

https://doi.org/10.1017/jfm.2014.531 Published online by Cambridge University Press

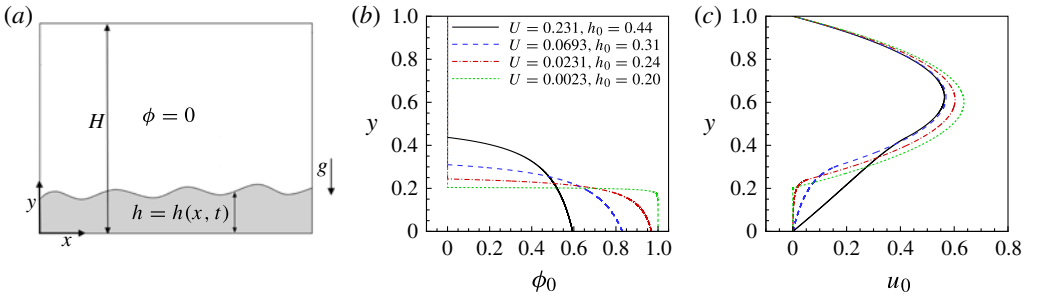


FIGURE 1. (Colour online) (*a*) The model of a sediment suspension flow in a channel of width H. The flow is induced by the pressure gradient $-\partial p/\partial x$ along the channel. The height of the interface between the clear fluid and the suspension is defined by $h(x, t)$. The volume fraction ϕ of particles is zero for $y > h(x, t)$, and it is maximum at the channel bed defined by $y = 0$. (*b*) The steady-state solution of the particle volume fraction. (*c*) The velocity profile of the suspension in the y direction for different values of 0.0023 m s^{-1} < U < 0.231 m s^{-1}. The results in panels (*b*) and (*c*) have been obtained using the following set of model parameters: $a = 72.1$ μm, $H = 4.33$ mm, $\rho_p = 1020$ kg m^{-3}, $\rho_f = 1000$ kg m^{-3}, $\mu_f = 0.001$ Pa s and $\phi_t = 0.2$. They correspond to $Re = (10, 100, 300, 1000)$ and $Sh = (0.0378, 0.378, 1.134, 3.78)$ for $U = (0.0023, 0.0231, 0.0693, 0.231)$, respectively.

particles. Figure 1(*a*) shows a schematic view of the channel, the sediment and the clear fluid above it. The x- and y-coordinates are parallel and normal to the channel centreline, respectively. Particles are deposited over the channel bed due to gravity, and at any position x and time t, the height of the sediment layer is measured by the function $h(x, t)$. The carrier fluid is still present in the sediment and feels the pressure gradient $\partial p/\partial x < 0$ along the channel. At the boundary between the clear fluid and the sediment we require $\phi = 0$. The stopping time of particles due to the drag force is assumed to be short (infinite-drag regime). Therefore, the particles and the carrier fluid have the same Eulerian velocity field $\boldsymbol{v} = u(x, y, t)\,\boldsymbol{e}_x + v(x, y, t)\,\boldsymbol{e}_y$, where $\boldsymbol{e}_x$ and $\boldsymbol{e}_y$ are unit base vectors in Cartesian coordinates. We normalize the physical quantities as $(\bar{x}, \bar{y}, \bar{u}, \bar{v}, \bar{t}, \bar{\phi}) = (x/H, y/H, u/U, v/U, t\,U/H, \phi/\phi_m)$, where U is the maximum velocity of Poiseuille flow inside the same channel but in the absence of spherical particles. For brevity, we will drop the overbar in our subsequent analysis, and all governing equations will be expressed in their normalized forms.

The continuity equation for the suspension reads

$$\rho_{,t} + \boldsymbol{\nabla} \cdot (\rho \boldsymbol{v}) = 0, \quad \boldsymbol{\nabla} = \boldsymbol{e}_x \frac{\partial}{\partial x} + \boldsymbol{e}_y \frac{\partial}{\partial y}, \tag{2.1}$$

where $\rho = (\rho_p/\rho_f)\phi_m\phi + (1 - \phi_m\phi)$ is the normalized density of the suspension and $(\cdot)_{,s} \equiv \partial(\cdot)/\partial s$. The subscripts p and f label the physical properties of the particle and fluid phases, respectively. We confine our study to suspensions with $|\rho_p - \rho_f|/\rho_f \ll 1$, which implies $\rho \approx \rho_f$. The continuity equation is thus reduced to $\boldsymbol{\nabla} \cdot \boldsymbol{v} = 0$. Let us denote the dynamic viscosity of the carrier fluid by μ_f, and introduce the channel Reynolds number $Re = \rho_f U H/\mu_f$. The momentum equations become

$$Re\left(u_{,t} + u\,u_{,x} + v\,u_{,y}\right) = \left[\mu(\phi)\left(u_{,y} + v_{,x}\right)\right]_{,y} + 2\left[\mu(\phi)u_{,x}\right]_{,x} - p_{,x}, \tag{2.2}$$

$$Re\left(v_{,t} + u\,v_{,x} + v\,v_{,y}\right) = \left[\mu(\phi)\left(u_{,y} + v_{,x}\right)\right]_{,x} + 2\left[\mu(\phi)v_{,y}\right]_{,y} - p_{,y} - \frac{gH^2}{\mu_f U}, \tag{2.3}$$

https://doi.org/10.1017/jfm.2014.531 Published online by Cambridge University Press

where g is the gravitational acceleration, p is the normalized pressure and $\mu(\phi)$ is the relative viscosity of the suspension with respect to clear fluid. We follow Phillips, Armstrong & Brown (1992) and set $\mu(\phi) = (1-\phi)^{-1.82}$ for a monodisperse suspension of spherical particles. We model the shear-induced migration of particles utilizing the diffusive flux of Cook (2008), which is a generalization of the phenomenological model of Phillips *et al.* (1992) to mixtures of negatively buoyant particles. The transport of particles due to the combined effects of shear-induced collisions and gravitational forces is thus described by

$$\phi_{,t} + (\boldsymbol{v}\cdot\boldsymbol{\nabla})\phi + \phi_m (a/H)^2 \boldsymbol{\nabla}\cdot\boldsymbol{J} = 0, \tag{2.4}$$

where the particle flux vector $\boldsymbol{J}$ is determined from

$$\boldsymbol{J} = -\left\{K_c \phi \begin{bmatrix} (\Gamma\phi)_{,x} \\ (\Gamma\phi)_{,y} \end{bmatrix} + K_v \phi^2 \Gamma \frac{\mu'(\phi)}{\mu(\phi)} \begin{bmatrix} \phi_{,x} \\ \phi_{,y} \end{bmatrix}\right\} - \frac{1}{\phi_m \mathscr{S}} \begin{bmatrix} 0 \\ \frac{\phi f(\phi)}{\mu(\phi)} \end{bmatrix}. \tag{2.5}$$

Here, a is the radius of the spherical particles and $\mathscr{S}$ is a dimensionless parameter defined as

$$\mathscr{S} = \frac{9\mu_f U}{2g(\rho_p - \rho_f)H^2} = \frac{9}{2}\frac{a}{H} Sh, \tag{2.6}$$

where Sh is the Shields parameter. The first two terms in (2.5) correspond to SID, which is controlled by the direct collision of particles. The last term in (2.5) models the effect of gravity on particle migration, with $f(\phi)$ being a hindrance function that takes into account the slowed gravity-induced deposition of particles as the particle concentration increases. The experimental work of Schaflinger, Acrivos & Zhang (1990) shows that $f(\phi) = 1 - \phi_m\phi$ is a reasonable model in the presence of a shear rate. The magnitude of the local shear rate Γ (e.g. Khoshnood & Jalali 2012) is

$$\Gamma = \left[|u_{,y}^2 + v_{,x}^2 + 2u_{,y}v_{,x} - 4u_{,x}v_{,y}|\right]^{1/2}. \tag{2.7}$$

The empirical constant coefficients K_c and K_v respectively show how the spatial gradients of $(\Gamma\phi)$ and μ affect the shear-induced migration. Following the experimental results of Phillips *et al.* (1992), we use $K_c = 0.41$ and $K_v = 0.62$. We have neglected the Brownian diffusion of particles by assuming that the Péclet number is large, $Pe \gg 1$. The boundary conditions at the channel walls include zero velocity and zero particle flux.

We assume that the particle volume fraction becomes zero at $y = h$, and obtain $\phi(x, h(x,t), t) = 0$. The total derivatives $\mathrm{D}\phi/\mathrm{D}t$ and $\mathrm{D}\phi/\mathrm{D}x$ should also vanish at the interface between the sediment and the clear fluid. Consequently,

$$\left[\phi_{,t} + h_{,t}\phi_{,y}\right]_{y=h} = 0, \quad \left[\phi_{,x} + h_{,x}\phi_{,y}\right]_{y=h} = 0. \tag{2.8a,b}$$

Substituting for $\phi_{,x}$ and $\phi_{,t}$ from (2.8) into (2.4) leads to

$$h_{,t} + u\,h_{,x} - v - \phi_m\,(a/H)^2\,(\boldsymbol{\nabla}\cdot\boldsymbol{J})\,/\phi_{,y} = 0 \quad \text{at } y = h, \tag{2.9}$$

which determines the evolution of $h(x,t)$. In (2.9), the term involving the divergence of the particle flux vector makes the interfacial waves of suspensions distinct from surface waves developing at the boundaries of simple viscous liquids.

https://doi.org/10.1017/jfm.2014.531 Published online by Cambridge University Press

2.1. *Steady-state streaming*

For a steady-state flow along the x direction, the partial derivatives of physical quantities with respect to x and t are zero, the sediment height remains constant and $v = 0$. We denote the steady-state velocity, pressure, sediment height and particle volume fraction by $\boldsymbol{v} = u_0(y)\boldsymbol{e}_x$, $p_0(x, y)$, h_0 and $\phi_0(y)$, respectively. The constant sediment height h_0 is determined from the total particle volume fraction $\phi_t = \int_0^{h_0} \phi_0(y)\mathrm{d}y$. The steady-state magnitude of the shear rate is computed from $\Gamma = |u_{0,y}|$, and the momentum and particle transport equations reduce to

$$\left[\mu(\phi_0)u_{0,y}\right]_{,y} - p_{0,x} = 0, \quad \frac{\rho_f H^2}{U\mu_f} g - p_{0,y} = 0, \tag{2.10a,b}$$

$$\left[\left(K_c\,|u_{0,y}|\phi_0\right)_{,y}\phi_0 + \frac{K_v\,\phi_0^2\,\mu_{,\phi}(\phi_0)\,|u_{0,y}|}{\mu(\phi_0)}\phi_{0,y}\right]_{,y} + \left[\frac{\phi_0(1-\phi_m\phi_0)}{\mu(\phi_0)\,\phi_m\mathscr{S}}\right]_{,y} = 0, \tag{2.11}$$

which are subject to the following boundary conditions:

$$u_0 = 0, \quad J_y = 0 \quad \text{at } y = 0,\, 1. \tag{2.12a,b}$$

Integration of (2.11) over y and imposition of the boundary conditions (2.12) yield $J_y(x, y, t) = 0$. The momentum equation in the y direction implies a linear pressure function in terms of y. Since $p_{0,x}$ is independent of y, one can integrate the momentum equation in the x direction to obtain

$$\Gamma_0 = |u_{0,y}| = |p_{0,x}\,y + B|/\mu(\phi_0), \tag{2.13}$$

where B is a to-be-determined constant. Let us define $F_1(\phi) = \phi\mu_{,\phi}(\phi)/\mu(\phi)$ and $F_2(\phi) = (1 - \phi_m\phi)/\mu(\phi)$. Substituting from (2.13) into $J_y = 0$, we obtain an ordinary differential equation (ODE) for the particle volume fraction:

$$\frac{\mathrm{d}\phi_0}{\mathrm{d}y} = \frac{1}{\Gamma_0}\frac{F_2(\phi_0)/(\phi_m\mathscr{S}) + K_c\,\phi_0\,p_{0,x}\,\mathrm{sgn}(u_{0,y})/\mu(\phi_0)}{K_c[1 - \phi_0\mu'(\phi_0)/\mu(\phi_0)] + K_v\,F_1(\phi_0)}, \tag{2.14}$$

with the boundary condition $\phi_0(h_0) = 0$. Equation (2.14) involves the two unknown parameters h_0 and B, which can be determined using (i) no-slip boundary conditions at the channel walls and (ii) the conservation of the total particle volume fraction ϕ_t. We find

$$\boldsymbol{f}(\boldsymbol{w}) = (f_1, f_2)^{\mathrm{T}} = \boldsymbol{0}, \quad \boldsymbol{w} = (h_0, B), \tag{2.15}$$

where

$$f_1(\boldsymbol{w}) = \int_0^1 \frac{p_{0,x}y + B}{\mu(\phi_0)}\,\mathrm{d}y = \int_0^1 u_{0,y}\,\mathrm{d}y = u_0(1) - u_0(0) = 0, \tag{2.16}$$

$$f_2(\boldsymbol{w}) = \phi_t - \int_0^{h_0} \phi_0(y)\mathrm{d}y = 0. \tag{2.17}$$

We use Newton's method to compute $\boldsymbol{w} = (h_0, B)$. Let $\boldsymbol{w}_n$ be the current approximate value of $\boldsymbol{w}$. Direct integration of (2.14) over y gives $\phi_{0,n}(y, \boldsymbol{w}_n)$, which is substituted into (2.15) to obtain the $(n + 1)$th approximation of the solution as $\boldsymbol{w}_{n+1} = \boldsymbol{w}_n - \boldsymbol{J}_f^{-1} \cdot \boldsymbol{f}(\boldsymbol{w}_n)$, where $\boldsymbol{J}_f$ is the Jacobian matrix corresponding to $\boldsymbol{f}$. Occasionally, Newton's method should be combined with bisection or secant techniques to guarantee the convergence to the root of (2.15).

https://doi.org/10.1017/jfm.2014.531 Published online by Cambridge University Press

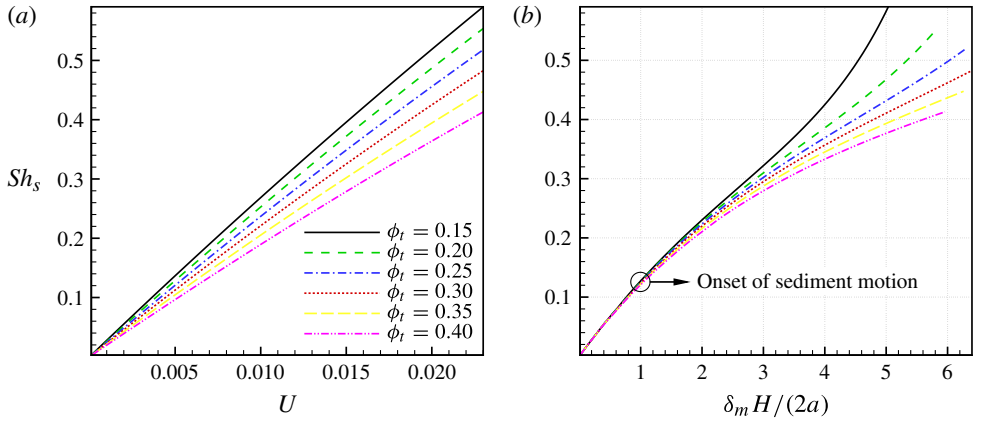


FIGURE 2. (Colour online) The variation of the Shields parameter Sh_s at the surface of the bed versus U (panel a) and $\delta_m H/(2a)$ (panel b). In both panels ϕ_t varies from 0.15 (dot-dot-dashed line) to 0.4 (solid line) with increments of 0.05. The critical Shields parameter Sh_c for the onset of sediment motion is computed by setting $\delta_m H/2a = 1$.

The steady-state solutions $\phi_0(y)$ and $u_0(y)$ depend on the dimensionless parameters $\mathscr{S}$ and ϕ_t. In our proceeding calculations we will set $p_{0,x} = -8$ so that $u_{0,max} = \max[u_0(y)]$ becomes unity as $\phi_t \to 0$. Figure 1(*b*,*c*) shows the steady-state profiles of $\phi_0(y)$ and $u_0(y)$ for different values of U. The model parameters are $a = 72.1$ μm, $H = 4.33$ mm, $\phi_t = 0.2$, $\rho_p = 1020$ kg m^{-3}, $\rho_f = 1000$ kg m^{-3} and $\mu_f = 0.001$ Pa s. These parameters yield the following set of dimensionless parameters: $a/H = 0.01667$, $Re = 4.33 \times 10^3\, U$ and $Sh = 16.35U$. It is seen that the sediment height varies proportional to the flow rate because shear forces that displace particles perpendicular to the flow direction dominate gravity forces. Moreover, for low flow rates the streaming velocity of the sediment drops significantly and particles settle with maximum concentration in the sediment layer. The velocity and concentration profiles reported in figure 1(*b*,*c*) resemble previous experimental and theoretical studies (Miskin *et al.* 1996; Aussillous *et al.* 2013).

The incipient motion of particles at the surface of the bed occurs for $Sh_s > Sh_c$ (Charru & Mouilleron-Arnould 2002; Ouriemi *et al.* 2007), where $Sh_s = \mu U u_{0,y}(h_0)/[2aHg(\rho_p - \rho_f)]$ is the Shields parameter at the surface of the bed and Sh_c is the critical Shields parameter for which the sheared sediment starts to move. Previous experimental studies have shown that $Sh_c \approx 0.12$, which is independent of the Reynolds number and the initial volume fraction of particles (Ouriemi *et al.* 2007). In order to quantify the onset of sediment motion, we have produced steady-state solutions for 0.001 m s^{-1} $< U <$ 0.023 m s^{-1} and for different values of ϕ_t. We have calculated the thickness δ_m of the mobile layer from $u_0(h_0 - \delta_m) = 0.01u_0(h_0)$. Figure 2(*a*,*b*) demonstrates the variation of Sh_s in terms of U and $\delta_m H/2a$ for several choices of ϕ_t. It is evident that Sh_s increases proportional to U. The sediment motion occurs when a monolayer of particles slides over the rest of the sediment. This roughly happens for $\delta_m H/2a \approx 1$, which according to figure 2(*b*) leads to $0.122 \lesssim Sh_c \lesssim 0.128$. This result is in harmony with the experimental results of Ouriemi *et al.* (2007).

2.2. *Perturbation theory and spectral analysis*

We are not aware of analytical solutions for the system of (2.2), (2.3), (2.4) and (2.9), and construct perturbation solutions to investigate the evolution of the interface

https://doi.org/10.1017/jfm.2014.531 Published online by Cambridge University Press

function $h(x, t)$. We define ϵ as a small perturbation parameter. The major difficulty in the perturbative analysis of sediment interfaces is that the formal series expansion

$$\phi = \phi_0(y) + \epsilon\phi_1(x, y, t) + O\left(\epsilon^2\right), \quad |\epsilon\phi_1/\phi_0| \ll 1, \tag{2.18a,b}$$

fails at $y = h(x, t)$ as we explain below. We assume that (2.18) represents the variation of the particle volume fraction as the interface is deformed, and set $h = h_0 + \epsilon h_1(x, t)$. At the interface we require

$$\phi(h) = \phi_0(h) + \epsilon\phi_1(x, h_0, t) + O\left(\epsilon^2\right) = 0. \tag{2.19}$$

For $h > h_0$ one has $\phi_0(h) = 0$, which implies $\phi_1(x, h_0, t) = 0$ up to the first-order terms in ϵ. For $h < h_0$, however, the steady-state volume fraction is non-zero, $\phi_0(h) > 0$, and we arrive at the inconsistent result $\phi_1(x, h_0, t) \approx -\phi_0(h)/\epsilon$. Here, we devise a perturbation theory that overcomes this problem. Let us disturb the velocity field and interface profile in the vicinity of their steady-state solutions as

$$u = u_0(y) + \epsilon u_1(x, y, t), \quad v = \epsilon v_1(x, y, t), \quad h = h_0 + \epsilon h_1(x, t), \tag{2.20a–c}$$

and assume the following analytical form for the particle volume fraction:

$$\phi = \phi_0\left(\frac{h_0}{h}y\right) + \epsilon\tilde{\phi}_1(x, y, t). \tag{2.21}$$

It is seen that $\phi(x, h, t) = \epsilon\tilde{\phi}_1(x, h_0, t) + O(\epsilon^2)$. In a linear perturbation analysis, $\tilde{\phi}_1$ is computed over the initial domain $0 \leqslant y \leqslant h_0$ and the boundary condition $\tilde{\phi}_1(x, h_0, t) = 0$ assures the fulfilment of the condition $\phi(h) = 0$ regardless of the sign of $\epsilon h_1(x, t)$. Substitution for h from (2.20) into (2.21) and keeping only the first-order terms in ϵ lead to

$$\phi = \phi_0(y) + \epsilon\phi_1(x, y, t), \quad \phi_1(x, y, t) = -\frac{y\phi_{0,y}}{h_0}h_1(x, t) + \tilde{\phi}_1(x, y, t), \tag{2.22}$$

which preserves the positivity of ϕ over the entire (x, y)-domain if $|\epsilon\phi_1| \ll \phi_0$. One may intuitively adopt the expansion

$$\phi = \phi_0 + \epsilon\phi_1, \quad \phi_1(h_0) = -h_1\phi_{0,y}(h_0), \tag{2.23a,b}$$

to describe the perturbations of particle volume fraction. Although this representation is identical to (2.22) up to the first-order terms in ϵ, its application becomes problematic while imposing boundary conditions at $y = h$. This is because we need to evaluate $\phi_{,y}$, which admits different values for $h > h_0$ and $h < h_0$ if (2.23) is applied. In our proposed method, however, the value of $\phi_{,y}(h)$ can be easily calculated by differentiating (2.21) with respect to y, and we only require to evaluate $\phi_{0,y}$ at the initial height of the interface: $y = h_0$.

By introducing the stream functions ψ^- and ψ^+ over the regions $0 \leqslant y \leqslant h_0$ and $h_0 < y \leqslant 1$, respectively, one can determine the perturbed velocity fields of the suspension and the clear fluid from $(\epsilon u_1^-, \epsilon v_1^-) = (\psi_{,y}^-, -\psi_{,x}^-)$ and $(\epsilon u_1^+, \epsilon v_1^+) = (\psi_{,y}^+, -\psi_{,x}^+)$. These assumptions satisfy the continuity equation automatically. Furthermore, taking the curl of the momentum equations replaces them by vorticity equations and eliminates the pressure p from our calculations.

By defining the operators

$$\nabla^2 = \boldsymbol{\nabla}\cdot\boldsymbol{\nabla} = (\cdot)_{,xx} + (\cdot)_{,yy}, \quad \blacktriangledown^2 = (\cdot)_{,yy} - (\cdot)_{,xx}, \tag{2.24a,b}$$

the perturbed governing equations read as follows.

https://doi.org/10.1017/jfm.2014.531 Published online by Cambridge University Press

(i) Vorticity equation for the suspension ($0 \leqslant y \leqslant h_0$):

$$\begin{aligned} &Re\left(\nabla^2\psi^-_{,t} + u_0\nabla^2\psi^-_{,x} - u_{0,yy}\psi^-_{,x}\right) \\ &\quad = \mu(\phi_0)\nabla^2\nabla^2\psi^- + 2\mu'(\phi_0)\phi_{0,y}\nabla^2\psi^-_{,y} + \left[\mu'(\phi_0)\phi_{0,y}\right]_{,y} \\ &\qquad \times \blacktriangledown^2\psi^- + \blacktriangledown^2\left[\mu'(\phi_0)u_{0,y}\phi_1\right]. \end{aligned} \tag{2.25}$$

(ii) Vorticity equation for the clear fluid ($h_0 < y \leqslant 1$):

$$Re\left(\nabla^2\psi^+_{,t} + u_0\nabla^2\psi^+_{,x} - u_{0,yy}\psi^+_{,x}\right) = \nabla^2\nabla^2\psi^+. \tag{2.26}$$

(iii) Particle transport equation:

$$\phi_{1,t} + u_0\phi_{1,x} - \phi_{0,y}\psi^-_{,x} + \phi_m\,(a/H)^2\nabla\cdot\boldsymbol{J}_1 = 0, \quad 0 \leqslant y \leqslant h_0. \tag{2.27}$$

(iv) Variation of the sediment height:

$$h_{1,t} + u_0h_{1,x} + \psi^-_{,x} - \phi_m\,(a/H)^2\frac{\nabla\cdot\boldsymbol{J}_1}{\phi_{0,y}} = 0 \quad \text{at } y = h_0. \tag{2.28}$$

Here, the components of the perturbed particle flux vector $\boldsymbol{J}_1 = (J_{1x}, J_{1y})$ are calculated from

$$J_{1x} = -K_c\phi_0(\Gamma_0\phi_1)_{,x} - K_c\phi_0^2\left[\mathrm{sgn}(u_{0,y})\,\blacktriangledown^2\psi^-\right]_{,x} - K_vF_3(\phi_0)\Gamma_0\phi_{1,x}, \tag{2.29}$$

$$\begin{aligned} J_{1y} = {} & -K_c\phi_0(\Gamma_0\phi_1)_{,y} - K_c\phi_0\left[\mathrm{sgn}(u_{0,y})\phi_0\,\blacktriangledown^2\psi^-\right]_{,y} - K_c(\Gamma_0\phi_0)_{,y}\phi_1 - \frac{F_{4,\phi}(\phi_0)}{\phi_m\mathscr{S}}\phi_1 \\ & - K_vF_3(\phi_0)\Gamma_0\phi_{1,y} - K_vF_3(\phi_0)\phi_{0,y}\,\mathrm{sgn}(u_{0,y})\,\blacktriangledown^2\psi^- - K_vF_{3,\phi}(\phi_0)\Gamma_0\phi_{0,y}\phi_1, \end{aligned} \tag{2.30}$$

with $F_3(\phi) = \phi F_1(\phi)$ and $F_4(\phi) = \phi F_2(\phi)$. Similar equations involving the vorticity of the suspension and the particle flux vector have been applied to Brownian suspensions in microchannels (Khoshnood & Jalali 2012). It is remarked that in the perturbed equations ϕ_1 is computed from (2.22). Equations (2.25)–(2.28) are coupled linear partial differential equations whose coefficients are functions of y. Therefore, the Fourier transforms of the perturbed equations are decoupled in the x-domain, and one can assume the following forms of the solutions:

$$\psi^{\pm}(x, y, t) = \Psi^{\pm}(y)\,\mathrm{e}^{\mathrm{i}kx - \mathrm{i}\omega t}, \quad h_1(x, t) = Y\,\mathrm{e}^{\mathrm{i}kx - \mathrm{i}\omega t}, \quad \tilde{\phi}_1 = \Phi(y)\,\mathrm{e}^{\mathrm{i}kx - \mathrm{i}\omega t}, \tag{2.31a–c}$$

where k is the wavenumber in the flow direction, $\omega = \Omega + \mathrm{i}s$ is the frequency of oscillations, Y is a constant amplitude and $\mathrm{i} = \sqrt{-1}$. Interface oscillations become unstable if $s > 0$. Substitution from (2.31) into (2.25)–(2.28) results in an eigenvalue problem as

$$-\mathrm{i}\omega\,Re\left(\Psi^-_{,yy} - k^2\Psi^-\right) + \mathscr{L}_{11}\Psi^- + \mathscr{L}_{13}\Phi + \mathscr{L}_{14}Y = 0, \quad 0 \leqslant y \leqslant h_0, \tag{2.32}$$

$$-\mathrm{i}\omega\,Re\left(\Psi^+_{,yy} - k^2\Psi^+\right) + \mathscr{L}_{21}\Psi^+ = 0, \quad h_0 < y \leqslant 1, \tag{2.33}$$

$$-\mathrm{i}\omega\left(\Phi - yh_0^{-1}\phi_{0,y}Y\right) + \mathscr{L}_{31}\Psi^- + \mathscr{L}_{33}\Phi + \mathscr{L}_{34}Y = 0, \quad 0 \leqslant y \leqslant h_0, \tag{2.34}$$

$$\left[-\mathrm{i}\omega + \mathrm{i}k\,u_0(h_0)\right]Y + \left[\mathscr{L}_{41}\Psi^-\right]_{y=h_0} + \left[\mathscr{L}_{43}\Phi\right]_{y=h_0} = 0, \tag{2.35}$$

where $\mathscr{L}_{ij}f = \sum_{m=0}^{M} c_{ijm}(y)\,\mathrm{d}^mf/\mathrm{d}y^m$ are linear differential operators with $c_{ijm}(y)$ being functions of y and model parameters; M ranges up to 4 and 2 if the operands are $\Psi^{\pm}$

https://doi.org/10.1017/jfm.2014.531 Published online by Cambridge University Press

and Φ, respectively. We therefore need 10 boundary conditions to solve the system of (2.32)–(2.35). Four conditions come from zero-velocity requirements at the walls of the channel:

$$u_1(x, 0, t) = v_1(x, 0, t) = 0 \rightarrow \Psi^-(0) = \Psi^-_{,y}(0) = 0, \tag{2.36}$$

$$u_1(x, 1, t) = v_1(x, 1, t) = 0 \rightarrow \Psi^+(1) = \Psi^+_{,y}(1) = 0. \tag{2.37}$$

The fifth boundary condition corresponds to zero volume fraction at $y = h$. We obtain

$$\phi(x, h, t) = \phi_0(h_0) + \epsilon\tilde{\phi}_1(x, h, t) = 0 \rightarrow \Phi(h_0) = 0, \tag{2.38}$$

up to the terms of $O(\epsilon)$. The sixth condition is associated with zero particle flux normal to the lower channel wall at $y = 0$:

$$J_{1y}(x, 0, t) = 0. \tag{2.39}$$

In this equation J_{1y} has been calculated using (2.30). The four remaining boundary conditions come from the continuity of physical quantities at the interface of the suspension and the clear fluid. They are (i) the continuity of the velocity field, (ii) the continuity of the shear stress and (iii) the continuity of the normal stress, which implies the continuity of the pressure field.

In the linear perturbation analysis, all boundary conditions at $y = h$ are evaluated for $y = h_0$ using a Taylor series expansion (Yih 1967). By defining $h^\pm = h + 0^\pm$, the continuity of the velocity vector at the interface implies

$$u_0(x, h^-, t) + \epsilon u_1(x, h^-, t) = u_0(x, h^+, t) + \epsilon u_1(x, h^+, t), \tag{2.40}$$

$$v_1(x, h^-, t) = v_1(x, h^+, t), \tag{2.41}$$

which can be expressed in terms of the amplitude functions Y and $\Psi^\pm(y)$ as

$$Y\left[u_{0,y}(h_0^+) - u_{0,y}(h_0^-)\right] + \left[\Psi^+_{,y}(h_0^+) - \Psi^-_{,y}(h_0^-)\right] = 0, \tag{2.42}$$

$$\Psi^+(h_0^+) - \Psi^-(h_0^-) = 0. \tag{2.43}$$

The steady-state solutions show that $u_0(y)$ and its first-order derivative are continuous functions at $y = h_0$, but higher-order derivatives are discontinuous. The boundary condition (2.42) can thus be simplified as

$$\Psi^+_{,y}(h_0^+) = \Psi^-_{,y}(h_0^-). \tag{2.44}$$

Since ϕ and $\mu(\phi)$ are continuous functions of y, the continuity of shear stress yields the continuity of $u_{,y}$ at the interface and we obtain

$$Y\left[u_{0,yy}(h_0^+) - u_{0,yy}(h_0^-)\right] + \left[\Psi^+_{,yy}(h_0^+) - \Psi^-_{,yy}(h_0^-)\right] = 0. \tag{2.45}$$

We assume a zero surface tension at the interface of the sediment because any particle–particle repulsions between the molecules of the clear fluid and the suspension, which cause interfacial tension, are relaxed by SID. Therefore, the pressure field remains almost continuous at $y = h(x, t)$:

$$p(x, h^+(x, t), t) = p(x, h^-(x, t), t), \tag{2.46}$$

$$p^-_{,x} + \epsilon h_{1,x} p^-_{,y} = p^+_{,x} + \epsilon h_{1,x} p^+_{,y}. \tag{2.47}$$

https://doi.org/10.1017/jfm.2014.531 Published online by Cambridge University Press

The functions $p_{0,x}$ and $p_{0,y}$ computed in the steady state are continuous at the interface. Consequently, (2.47) yields the continuity of $p_{,x}$ up to the first-order terms in ϵ. The value of $p_{,x}$ can be determined using the momentum equation (2.2),

$$\begin{aligned}&\left[Re(u_{,t}+uu_{,x}+vu_{,y})-[\mu(\phi)(u_{,y}+v_{,x})]_{,y}-2[\mu(\phi)u_{,x}]\right]_{y=h^-}\\&\quad=\left[Re(u_{,t}+uu_{,x}+vu_{,y})-[(u_{,y}+v_{,x})]_{,y}-2[u_{,x}]\right]_{y=h^+}.\end{aligned}\tag{2.48}$$

Using the identity $\phi(h)=0$ and the continuity of the quantities u, $u_{,y}$, $u_{,x}$, $u_{,xx}$, v and $v_{,xy}$ at $y=h$, (2.48) is simplified to

$$\left[u_{,yy}+\mu'(0)\phi_{,y}(u_{,y}+v_{,x})+2\mu'(0)\phi_{,x}u_{,x}\right]_{y=h^-}=\left[u_{,yy}\right]_{y=h^+}.\tag{2.49}$$

Substituting for ϕ, u and v from (2.21) and (2.20) into (2.49), and using the first-order approximation of quantities in the vicinity of $y=h_0$, the boundary condition associated with the continuity of the pressure field becomes

$$\begin{aligned}&\left[\Psi^+_{,yyy}(h_0^+)-\Psi^-_{,yyy}(h_0^-)\right]+Y\left[u_{0,yyy}(h_0^+)-u_{0,yyy}(h_0^-)\right]\\&\quad-\mu'(0)[\phi_{0,y}(\Psi^-_{,yy}+k^2\Psi^-+u_{0,yy}Y-u_{0,y}Y/h_0)+u_{0,y}\Phi_{,y}]_{y=h_0^-}=0.\end{aligned}\tag{2.50}$$

We adopt a Chebyshev tau method (Dongarra, Straughan & Walker 1996) and expand the functions $\Psi^{\pm}(y)$ and $\Phi(y)$ as (see also Khoshnood & Jalali 2012)

$$\Psi^{\pm}(y)=\sum_{i=0}^{N+4}P_i^{\pm}\,T_i(y^{\pm}),\qquad \Phi(y)=\sum_{i=0}^{N+2}Q_i\,T_i(y^-),\tag{2.51a,b}$$

where T_i are Chebyshev functions, $y^-=2y/h_0-1$ and $y^+=2y/(1-h_0)-(1+h_0)/(1-h_0)$. It is seen that $-1\leqslant y^{\pm}\leqslant+1$. We collect all unknown variables $P_i^{\pm}$ and Q_i in a single vector z, and introduce the new unknowns τ_i ($i=1,2,\ldots,10$) associated with the ten boundary conditions. The weighted residual forms of (2.32)–(2.34) together with the boundary conditions and the algebraic equation (2.35) give a linear eigensystem $\boldsymbol{A}\cdot z=\omega\boldsymbol{B}\cdot z$, where $\boldsymbol{A}$ and $\boldsymbol{B}$ are complex matrices. The τ_i are determined after computing ω and its corresponding eigenvector z. One can tag and remove spurious modes from the eigenspectrum by looking at the values of τ_i. In our calculations we tag a mode as spurious if $\max\{|\tau_i|,\,1\leqslant i\leqslant 10\}>0.1\,\max\{|z_i|,\,0\leqslant i\leqslant 3N+13\}$. We have tested our code by finding the eigenfrequencies of the Orr–Sommerfeld equation (Orszag 1971).

3. Unstable interfacial waves

We start with $N=30$ in (2.51) and increase the number of Chebyshev functions until the eigenspectrum of ω converges. In most cases, we need $N\leqslant 80$ to guarantee the convergence of eigenvalues within 0.5 % error. Equations (2.32)–(2.35) involve the four dimensionless parameters Re, a/H, ϕ_t and $\mathscr{S}=(9a/2H)Sh$. We have identified the fundamental mode, whose imaginary part s is the largest in the spectrum, and plotted the variations of its growth/decay rate in figure 3(*a–d*) versus the wavenumber k and model parameters. The fundamental mode, regardless of its stability nature, is an interfacial Kelvin–Helmholtz (K–H)-type wave (see figure 5). A discontinuity in the tail slope of certain $s(k)$ profiles occurs when the decay rate of the K–H mode becomes the second largest s in the spectrum. To better understand this behaviour, the value of s for the secondary mode has been plotted in figure 3(*b*) for $Sh=0.453$. The secondary mode becomes unstable only for unphysical waves whose wavelengths are extremely short ($k\gg 1$) and comparable with the diameter of the suspension particles.

https://doi.org/10.1017/jfm.2014.531 Published online by Cambridge University Press

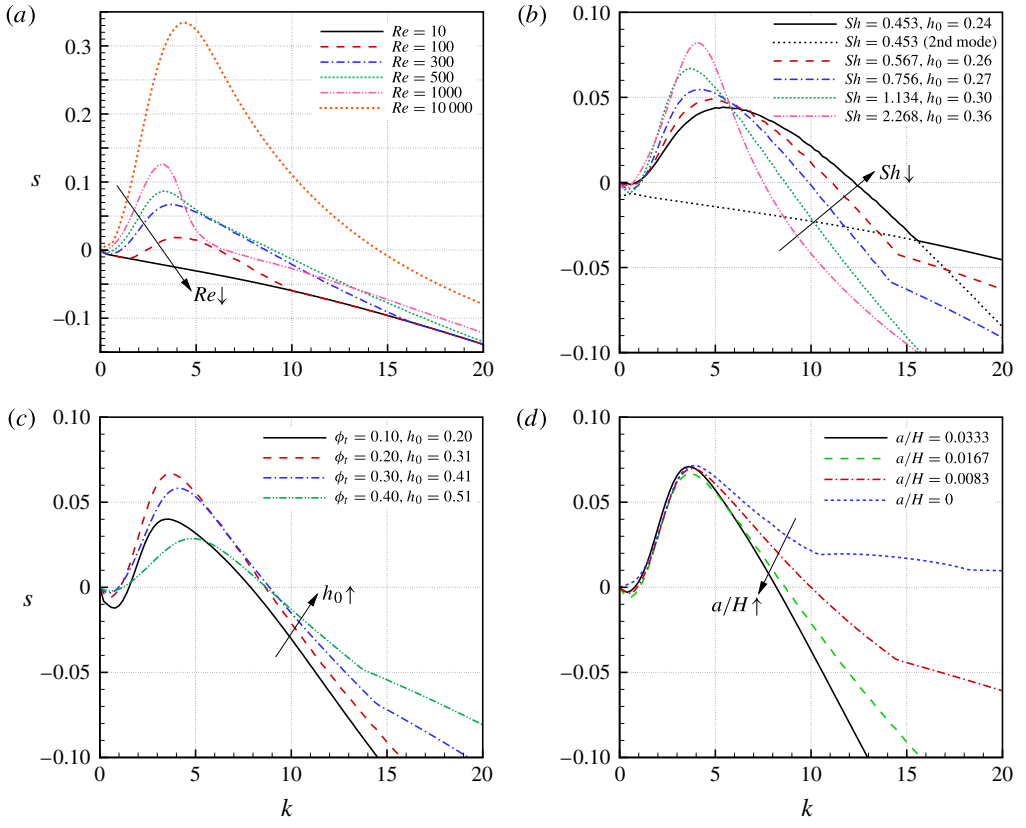


FIGURE 3. (Colour online) The growth/decay rate s of the fundamental mode as a function of the wavenumber k. Panels (*a*)–(*d*) demonstrate, respectively, the effects of the Reynolds number, the Shields number, the total particle volume fraction ϕ_t and the dimensionless particle radius a/H on the mode growth, while other parameters are fixed: (*a*) $Sh = 1.134$, $\phi_t = 0.19$, $a/H = 0.0167$ and $h_0 = 0.3$; (*b*) $Re = 300$, $\phi_t = 0.19$ and $a/H = 0.0167$; (*c*) $Re = 300$, $Sh = 1.134$ and $a/H = 0.0167$; (*d*) $Re = 300$, $\mathscr{S} = 0.0042$ and $\phi_t = 0.19$. The width of the channel, H, is fixed and we have varied the particle radius a.

Our secondary mode is similar to the internal mode reported for the flow of two immiscible fluids (Yiantsios & Higgins 1988). It is worth noting that the variation of the sediment height is tiny for short-wavelength secondary modes: $|Y|/\max(|z|) \ll 1$.

Figure 3(*a*) shows the profile of $s(k)$ as the Reynolds number is varied. Increasing Re has a remarkable destabilizing effect on the fundamental mode. It is seen that interfacial instabilities do not occur for $Re \lesssim 10$. This finding is consistent with the experimental observations of Ouriemi, Aussillous & Guazzelli (2009): a moving flat bed, small dunes, vortex dunes and sinusoidal dunes develop in sediment pipe flow as the flow rate, and therefore the Reynolds number, is increased. The critical Reynolds number Re_{cr} for the formation of small dunes varies between 30 and 140 depending on the experimental set-up. Schaflinger (1994) has also reported $Re_{cr} \approx 100$ for ripple formation in two-dimensional experiments of Hagen–Poiseuille resuspension flow over a monolayer bed of particles. In figure 4, we have used the linear perturbation analysis of § 2.2 and plotted the variation of Re_{cr} and its

https://doi.org/10.1017/jfm.2014.531 Published online by Cambridge University Press

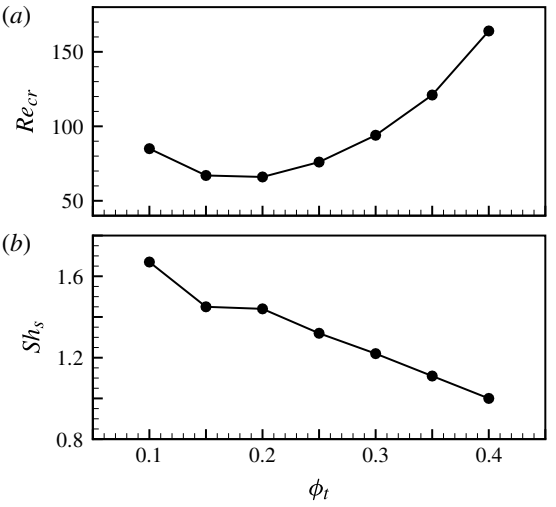


FIGURE 4. The variation of the critical Reynolds number (a) and its corresponding Shields number Sh_s at the interface (b) versus ϕ_t. We have chosen $Sh = 1.134$ and $a/H = 0.0167$.

corresponding Shields number Sh_s at the surface of the bed, in terms of the total particle volume fraction ϕ_t. We find that the fundamental K–H mode becomes unstable for $Re > Re_{cr}$, and the critical Reynolds number varies over the interval $65 < Re_{cr} < 160$ when the dimensionless parameters Sh and a/H are respectively set to 1.134 and 0.0167. Although there is qualitative agreement between this theoretical prediction and experimental measurements (Schaflinger 1994; Ouriemi *et al.* 2009), it is impossible to make a precise match due to the existence of a settled layer in the work of Ouriemi *et al.* (2009) and low values of $h_0 = 2a/H$ in Schaflinger (1994).

According to figure 3(a), by increasing Re the fundamental mode becomes unstable over a wider range of k, with some exceptions near $Re \approx 1000$. Moreover, the wavelength of the fastest growing mode, associated with the peak of the $s(k)$ curve, increases proportional to Re until we enter the turbulent regime with $Re \gtrsim 5000$. A similar behaviour has been reported in Schaflinger (1994) and Kuru *et al.* (1995). These investigators increased Re by controlling the flow rate, which also boosts the Shields number. In our analysis, however, we changed Re by keeping other dimensionless parameters constant.

The Shields number has a remarkable influence on the functional form of $s(k)$ for the fundamental mode, as seen in figure 3(b). By decreasing Sh, the particle phase becomes more concentrated in the steady state, and the sediment height h_0 decreases. The maximum value of $s(k)$ decreases proportional to Sh, indicating the stabilizing effect of the gravity force. Strong interfacial instabilities reported in the experiments of Schaflinger (1994) for large Shields numbers confirm our theoretical results. Decreasing Sh, however, destabilizes the K–H mode over shorter wavelengths (larger values of k). For very small values of Sh, particles are packed in the sediment with the maximum volume fraction, and the vertical profile of ϕ experiences steep changes at the interface (see figure 1c). Our eigenvalue solver does not converge well in such extreme circumstances. Large values of ϕ_t lead to sharp changes in the steady-state velocity and concentration profiles near the interface, enhance the viscosity stratification effect and destabilize the interface. Nevertheless, figure 3(c) shows that the largest growth rate of the fundamental mode appears for intermediate

https://doi.org/10.1017/jfm.2014.531 Published online by Cambridge University Press

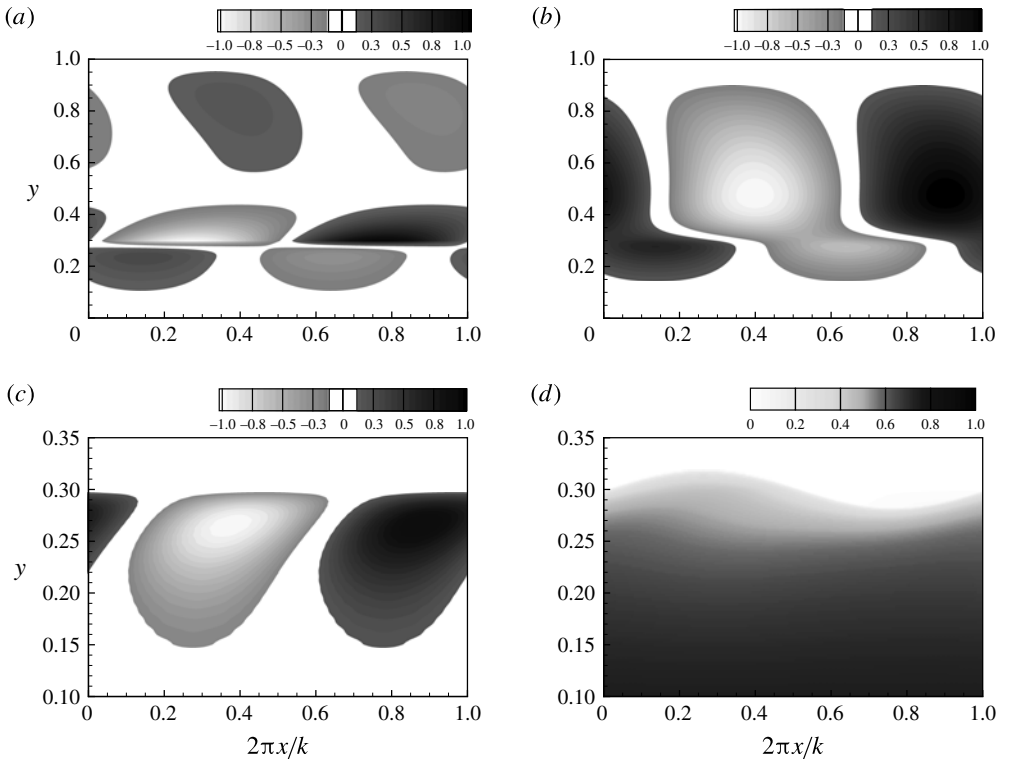


FIGURE 5. The fastest growing mode of the model with $Re = 300$ in figure 3(*a*). The eigenfrequency of the mode is $\omega = 0.66 + 0.067\,\mathrm{i}$, which corresponds to the wavenumber $k = 3.6$. Panels (*a*), (*b*) and (*c*) show the contours of u_1, v_1 and $\tilde{\phi}_1$, respectively. (*d*) The pattern of ϕ at $t = 0$ for $\epsilon = 0.01$.

values $\phi_t \approx 0.2$, which correspond to the lowest limit of Re_{cr} in figure 4. A reasonable explanation for this observation is that increasing ϕ_t beyond ≈ 0.2 raises the sediment height h_0 and displaces the interface towards minimum shear zones near the channel centreline. Consequently, the K–H mode cannot be easily triggered.

The steady-state solutions do not depend on the size of particles because a does not appear in (2.14). The perturbed dynamics, however, is controlled by the parameter $(a/H)^2$ in (2.27) and (2.28). The variation of s in terms of k and a/H has been plotted in figure 3(*d*), which shows that SID efficiently damps short-wavelength K–H modes: the profile of $s(k)$ falls off rapidly as the particle radius in increased. If one turns off SID by setting $a/H = 0$, the instability will occur for all wavenumbers. It is obvious that in the limit of $2\pi/k \to 4a/H$, particle–particle collisions destroy any developing interfacial wave. It should be noted that the fastest growing mode in figure 3(*d*), with $k \approx 3.5$ and $s \approx 0.08$, is not affected by the size of particles because of its long wavelength. This is in harmony with the experiments of Kuru *et al.* (1995).

The dash-dotted line in figure 3(*a*) shows the variation of $s(k)$ for a model with $Re = 300$. The fastest growing mode of this model occurs for $k = 3.6$. The eigenfrequency of this fast mode is $\omega = 0.66 + 0.067\,\mathrm{i}$, the associated mode shapes of which are demonstrated in figure 5. We have plotted the contours of u_1, v_1, $\tilde{\phi}_1$ and ϕ at $t = 0$ for $\epsilon = 0.01$. It is seen that the particle concentration and the components of the streaming velocity are strongly disturbed near the interface.

https://doi.org/10.1017/jfm.2014.531 Published online by Cambridge University Press

4. Conclusions

The only experimental works in the literature with flow geometry, particle types and sediment properties similar to our theoretical model were conducted by Schaflinger (1994) and Schaflinger, Acrivos & Stibi (1995). These investigators do not provide experimentally measured values of the eigenfrequency ω, and their observed unstable interfaces have been deformed in the third dimension (e.g. Schaflinger 1994, figure 10). Therefore, an accurate comparison of our theoretical results with their observations is not feasible. Nonetheless, we can still compare the ranges of critical wavenumbers given h_0 and Re. It should be noted that ϕ_t and h_0 are correlated. The variation of $s(k)$ in figure 3(*b*,*c*) shows that for sediment heights $0.2 \lesssim h_0 \lesssim 0.5$ and with $Re \approx 300$, the wavenumber of the most unstable mode varies over the range $3 \lesssim k \lesssim 6$, which is consistent with the experimental wavelengths reported in table 1 and figure 5 of Schaflinger (1994).

Our work is distinct from previous theoretical studies in two aspects: (i) we take into account non-homogeneities in the particle concentration profiles in both the steady and the perturbed states; (ii) we model SID at the interface by perturbing the magnitude of the local shear rate. The positivity of the particle volume fraction is preserved using our new perturbation technique. For most models, we found a fundamental K–H mode whose stability was investigated by varying the model parameters and the wavelength of interface deformations. We showed that while acceleration terms have a destabilizing effect on interfacial waves, the gravity force and SID tend to stabilize such waves. Damping of short-wavelength interfacial oscillations is a remarkable consequence of SID and cannot be understood in the framework of Schaflinger (1994). Another notable finding of this study was the minimum of the $Re_{cr}(\phi_t)$ curve in figure 4, which shows the existence of a critical total volume fraction; this determines the highest Re that a sediment of spherical particles can tolerate before its interface develops an unstable K–H mode.

Acknowledgements

We thank A. Khoshnood for her valuable discussions and illuminating comments. M.A.J. thanks the Center for Integrative Planetary Science at the University of California, Berkeley, for their support. We also thank the anonymous referees for their useful comments.

REFERENCES

AUSSILLOUS, P., CHAUCHAT, J., PAILHA, M., MÉDALE, M. & GUAZZELLI, M. 2013 Investigation of the mobile granular layer in bedload transport by laminar shearing flows. *J. Fluid Mech.* **736**, 594–615.

CHARRU, F. & MOUILLERON-ARNOULD, H. 2002 Instability of a bed of particles sheared by a viscous flow. *J. Fluid Mech.* **452**, 303–323.

COOK, B. P. 2008 Theory for particle settling and shear-induced migration in thin-film liquid flow. *Phys. Rev.* E **78**, 045303(R).

DONGARRA, J. J., STRAUGHAN, B. & WALKER, D. W. 1996 Chebyshev tau/QZ algorithm methods for calculating spectra of hydrodynamic stability problems. *J. Appl. Numer. Math.* **22**, 399–435.

GOVINDARAJAN, R. 2004 Effect of miscibility on the linear instability of two-fluid channel flow. *Intl J. Multiphase Flow* **30** (10), 1177–1192.

HOOPER, A. P. & BOYD, W. G. C. 1983 Shear-flow instability at the interface between two viscous fluids. *J. Fluid Mech.* **128**, 507–528.

https://doi.org/10.1017/jfm.2014.531 Published online by Cambridge University Press

KHOSHNOOD, A. & JALALI, M. A. 2012 Long-lived and unstable modes of Brownian suspensions in microchannels. *J. Fluid Mech.* **701**, 407–418.

KOUAKOU, K. K. J. & LAGRÉE, P. Y. 2005 Stability of an erodible bed in various shear flows. *Eur. Phys. J.* **47**, 115–125.

KURU, W. C., LEIGHTON, D. T. & MCCREADY, M. J. 1995 Formation of waves on a horizontal erodible bed of particles. *Intl J. Multiphase Flow* **21** (6), 1123–1140.

LANGLOIS, V. & VALANCE, A. 2007 Initiation and evolution of current ripples on a flat sand bed under turbulent water flow. *Eur. Phys. J.* E **22**, 201–208.

LENOBLE, M., SNABRE, P. & POULIGNY, B. 2005 The flow of a very concentrated slurry in a parallel-plate device: influence of gravity. *Phys. Fluids* **17** (7), 073303.

MALEKI, M., PACHECO, H., SUÁREZ, C. R. & CLÉMENT, E. 2009 Interfacial instability of a confined suspension under oscillating shear. In *Traffic and Granular Flow '07*, pp. 621–627. Springer.

MISKIN, I., ELLIOTT, L. & INGHAM, D. B. 1999 Stability in a fully-developed two-dimensional resuspension flow. *Intl J. Multiphase Flow* **25** (3), 501–530.

MISKIN, I., ELLIOTT, L., INGHAM, D. B. & HOMMAND, P. S. 1996 Steady suspension flows into two-dimensional horizontal and inclined channels. *Intl J. Multiphase Flow* **22** (6), 123–1246.

NORMAN, J. T., NAYAK, H. V. & BONNECAZE, R. T. 2005 Migration of buoyant particles in low-Reynolds-number pressure-driven flows. *J. Fluid Mech.* **523**, 1–35.

ORSZAG, S. A. 1971 Accurate solution of the Orr–Sommerfeld stability equation. *J. Fluid Mech.* **50**, 689–703.

OURIEMI, M., AUSSILLOUS, P. & GUAZZELLI, E. 2009 Sediment dynamics. Part 2. Dune formation in pipe flow. *J. Fluid Mech.* **636**, 321–336.

OURIEMI, M., AUSSILLOUS, P., MEDALE, M., PEYSSON, Y. & GUAZZELLI, E. 2007 Determination of the critical Shields number for particle erosion. *Phys. Fluids* **19**, 061706.

PAPISTA, E., DIMITRAKIS, D. & YIANTSIOS, S. G. 2011 Direct numerical simulation of incipient sediment motion and hydraulic conveying. *Ind. Engng Chem. Res.* **50** (2), 630–638.

PHILLIPS, R. J., ARMSTRONG, R. C. & BROWN, R. A. 1992 A constitutive equation for concentrated suspensions that accounts for shear-induced particle migration. *Phys. Fluids* **4**, 30–40.

SCHAFLINGER, U. 1994 Interfacial instabilities in a stratified flow of two superposed fluids. *Fluid Dyn. Res.* **13** (6), 299–316.

SCHAFLINGER, U., ACRIVOS, A. & STIBI, H. 1995 An experimental study of viscous resuspension in a pressure-driven plane channel flow. *Intl J. Multiphase Flow* **21** (4), 693–704.

SCHAFLINGER, U., ACRIVOS, A. & ZHANG, K. 1990 Viscous resuspension of a sediment within a laminar and stratified flow. *Intl J. Multiphase Flow* **16** (4), 567–578.

TALON, L. & MEIBURG, E. 2011 Plane Poiseuille flow of miscible layers with different viscosities: instabilities in the Stokes flow regime. *J. Fluid Mech.* **686**, 484–506.

VALANCE, A. & LANGLOIS, V. 2005 Ripple formation over a sand bed submitted to a laminar shear flow. *Eur. Phys. J.* B **43** (2), 283–294.

YIANTSIOS, S. G. & HIGGINS, B. G. 1988 Linear stability of plane Poiseuille flow of two superposed fluids. *Phys. Fluids* **31**, 3225–3238.

YIH, C. S. 1967 Instability due to viscosity stratification. *J. Fluid Mech.* **27** (2), 337–352.

ZHANG, K., ACRIVOS, A. & SCHAFLINGER, U. 1992 Stability in a two-dimensional Hagen–Poiseuille resuspension flow. *Intl J. Multiphase Flow* **18** (1), 51–63.

https://doi.org/10.1017/jfm.2014.531 Published online by Cambridge University Press